Matrix stiffness and stress relaxation regulate osteogenesis through histone demethylases KDM4B and KDM6B

Ian M. Tayler[a], Amy Zhu[a], Abhishek Sharma[b], Neha Saxena[c], Siddharth S. Dey[c,d], and Ryan S. Stowers[b,d,*]

[a]Department of Molecular, Cellular and Developmental Biology, University of California, Santa Barbara, Santa Barbara, CA 93106; [b]Department of Mechanical Engineering, University of California, Santa Barbara, Santa Barbara, CA 93106; [c]Department of Chemical Engineering, University of California, Santa Barbara, Santa Barbara, CA 93106; [d]Department of Bioengineering, University of California, Santa Barbara, Santa Barbara, CA 93106

ABSTRACT **Stem cells sense biophysical cues within their extracellular microenvironment and respond via mechanotransduction signaling pathways that induce changes in gene expression and associated cell fate outcomes. Histone-modifying enzymes are known to drive stem cell differentiation through changes in chromatin accessibility, but little is understood as to how extracellular matrix (ECM) mechanics regulate epigenomic remodeling. Here, we utilized alginate hydrogels with tunable mechanical properties to investigate the role of both matrix stiffness and stress relaxation on histone demethylase expression and activity during osteogenic differentiation of human bone marrow-derived mesenchymal stem cells (hBMSCs). Our results revealed that the expression of two histone demethylases, KDM4B and KDM6B, was upregulated during osteogenesis in response to stiff and fast stress-relaxing matrix conditions. Additionally, CUT&Tag profiling coupled with RNA-sequencing demonstrated that repressive histone methylation was decreased at osteogenic-specific loci in stiff, fast-relaxing matrices. Further, inhibition of mechanotransduction signaling pathways reduced expression of KDM4B and KDM6B and hindered osteogenic differentiation overall. Interestingly, phosphorylation of SMAD 1/5/8 increased in cells cultured in stiff, stress-relaxing matrices, and pharmacological inhibition of SMAD 1/5/8 activation reduced expression of KDM4B and KDM6B. Together, our results establish novel impacts of stem cell mechanotransduction signaling events that promote osteogenesis through epigenetic remodeling.**

SIGNIFICANCE STATEMENT

- Bone marrow-derived mesenchymal stem cells (BMSCs) differentiate into osteoblasts in response to extracellular matrix (ECM) stiffness and stress relaxation. Histone demethylases KDM4B and KDM6B are known to regulate osteogenesis, but it is unclear how ECM mechanics induce epigenetic changes during differentiation.
- This study identified that stiff, fast-relaxing hydrogel matrices upregulated KDM4B and KDM6B during osteogenesis and that inhibition of mechanosignaling reduced their expression.
- These findings underscore how ECM mechanics are linked to epigenetic regulation of stem cells. Understanding how these signaling pathways guide stem cell fate is essential for future applications in disease modeling and regenerative medicine.

Monitoring Editor
Xuebiao Yao
University of Science and Technology of China

Received: Jul 17, 2025
Revised: Feb 6, 2026
Accepted: Mar 5, 2026

INTRODUCTION

Bone marrow-derived mesenchymal stem cells (BMSCs) are multipotent, mechanosensitive progenitors capable of differentiating into numerous cell types, including chondrocytes, adipocytes, and osteoblasts. During bone remodeling and fracture repair, BMSCs undergo osteogenic differentiation in response to sensing microenvironmental mechanical properties (Darnell *et al.*, 2017; Duan and Lu, 2021; Woloszyk *et al.*, 2022). In vitro experiments have shown that extracellular matrix (ECM) mechanical properties such as stiffness and stress relaxation regulate gene expression (Hwang *et al.*, 2015; Darnell *et al.*, 2018b) and ultimately stem cell differentiation through activation of mechanotransduction pathways (Engler *et al.*, 2006; Huebsch *et al.*, 2010; Parekh *et al.*, 2011; Chaudhuri *et al.*, 2016; Lee *et al.*, 2019). During osteogenesis, mechanosignaling emanates from integrin-based adhesion complexes and mechanically-sensitive ion channels to induce cytoskeletal remodeling, drive actomyosin contractility, and activate downstream signaling pathways such as RhoA, PI3K, and YAP/TAZ. (Fujita *et al.*, 2004; McBeath *et al.*, 2004; Taubenberger *et al.*, 2010; Huang *et al.*, 2023; Liu *et al.*, 2023; Li *et al.*, 2025). Intriguingly, it has become increasingly evident that ECM mechanics can induce epigenetic remodeling via cytoskeletal mechanotransduction to alter cellular phenotypes (Downing *et al.*, 2013; Stowers *et al.*, 2019; Jang *et al.*, 2021; Wu *et al.*, 2025). However, it remains unclear whether mechanically induced osteogenesis is influenced by epigenetic remodeling.

Osteogenesis is regulated through canonical bone morphogenetic protein (BMP) signaling via BMP receptor phosphorylation of SMAD 1/5/8 transcription factors, which translocate to the nucleus and facilitate osteogenic gene expression (Rahman *et al.*, 2015; Wu *et al.*, 2016). In concert with canonical BMP-SMAD signaling, BMSC lineage specification occurs through associated changes in gene expression that are ultimately regulated by chromatin accessibility (Huang *et al.*, 2015; Kanazawa *et al.*, 2021; Walewska *et al.*, 2023; Zhu *et al.*, 2024). These changes in accessibility are often governed by histone-modifying enzymes that chemically modify the N-terminal tails of histone subunits, commonly by acetylation or methylation, to enhance or repress gene transcription. Previous work has demonstrated that osteogenesis is epigenetically regulated through two lysine-specific histone demethylases, KDM4B and KDM6B, that are essential for osteogenic differentiation (Ye *et al.*, 2012; Xu *et al.*, 2013; Deng *et al.*, 2022). Expression of KDM4B and KDM6B is upregulated in BMSCs upon treatment with BMP 4/7 (Ye *et al.*, 2012), and the loss of their expression significantly decreases osteogenic differentiation. The demethylases KDM4B and KDM6B function at H3K9me3 and H3K27me3 sites, respectively, to coordinate the de-repression of key osteogenic genes (Ye *et al.*, 2012; Xu *et al.*, 2013; Deng *et al.*, 2022). However, it is not well understood how matrix mechanics regulate epigenetic state transitions in BMSCs during osteogenic differentiation, or whether KDM4B or KDM6B are mechanoresponsive during this lineage commitment.

In the present study, we aimed to determine how matrix mechanics impact the expression and activity of KDM4B and KDM6B in the context of mechanically induced osteogenic differentiation of human BMSCs (hBMSCs). We utilized a mechanically tunable, three-dimensional (3D) alginate hydrogel cell culture platform with independently tunable stiffness and stress relaxation rates. We have identified that stiffness and stress relaxation both regulate the expression of KDM4B and KDM6B and downstream hallmarks of early osteogenic differentiation. By encapsulating hBMSCs in these hydrogel networks, we delineated the combined effects of stiffness and stress relaxation to investigate how mechanotransduction signaling impacts epigenetic changes during osteogenesis. Here, we describe a novel function for the histone modifiers KDM4B and KDM6B and demonstrate that they are dependent on both mechanotransduction pathways and SMAD 1/5/8 signaling in 3D matrices. Our work provides further insight into how the cellular microenvironment impacts the lineage specification of mechanosensitive stem cells.

RESULTS

Hydrogel stiffness and stress relaxation rate regulate osteogenesis in 3D

To determine the influence of ECM mechanics on epigenetic changes during early osteogenic differentiation, we utilized an alginate hydrogel system that enables independent tuning of both matrix elastic modulus and stress relaxation rate (Figure 1A). Hydrogel crosslinking densities were tuned by varying the concentration of calcium to achieve elastic moduli of 20 kPa (stiff) or 3 kPa (soft); (Figure 1B). These elastic moduli were selected based on previous reports identifying stiffness-mediated osteogenic differentiation of MSCs in 3D (Huebsch *et al.*, 2010; Chaudhuri *et al.*, 2016). The hydrogel stress relaxation rates were tuned independently of stiffness by using alginates of varied molecular weights (Figure 1, C–D), and by conjugation of polyethylene glycol (PEG) to low molecular weight alginate polymers via carbodiimide chemistry (Nam *et al.*, 2019). Additionally, the RGD adhesion motif was then coupled to all alginate polymers as previously described (Rowley *et al.*, 1999) at a final concentration of 1,500 μM.

After characterizing the mechanical parameters of our hydrogel-based cell culture system, hBMSCs were encapsulated in alginate matrices and cultured for 7 days in osteogenic differentiation media. In line with previous studies (Chaudhuri *et al.*, 2016; Lee *et al.*, 2019), the cells in stiff, fast-relaxing matrices exhibited significantly more osteogenesis, assessed by the proportion of cells that stained positive for alkaline phosphatase (ALP), compared with softer or slower-relaxing hydrogel conditions (Figure 1E). Further analysis of early osteogenic differentiation markers by quantitative polymerase chain reaction (qPCR) revealed that cells cultured in stiff, fast-relaxing matrices displayed significantly greater gene expression of RUNX2, ALP, Collagen 1a1, and Osteocalcin compared with all other mechanical conditions (Figure 1F). We next sought to identify the ECM-mediated signaling pathways contributing to the hBMSCs' differential response to matrix stiffness and stress relaxation cues, both of which are known to promote osteogenic differentiation (Chaudhuri *et al.*, 2016; Darnell *et al.*, 2017; Lee *et al.*, 2019). In particular, integrin signaling and focal

This article was published online ahead of print in MBoC in Press (http://www.molbiolcell.org/cgi/doi/10.1091/mbc.E25-07-0331) on March 11, 2026.

Author contributions: I.T, S.S.D, and R.S.S. conceived and designed the experiments. I.T., A.Z., A.S., and N.S. performed the experiments. I.T., A.Z., A.S., and N.S. analyzed the data. I.T. and R.S. drafted the article. I.T., A.Z., A.S., and N.S. prepared the digital images.

Conflicts of interest: The authors declare no competing financial interest.

*Address correspondence to: Ryan S. Stowers (rstowers@ucsb.edu).

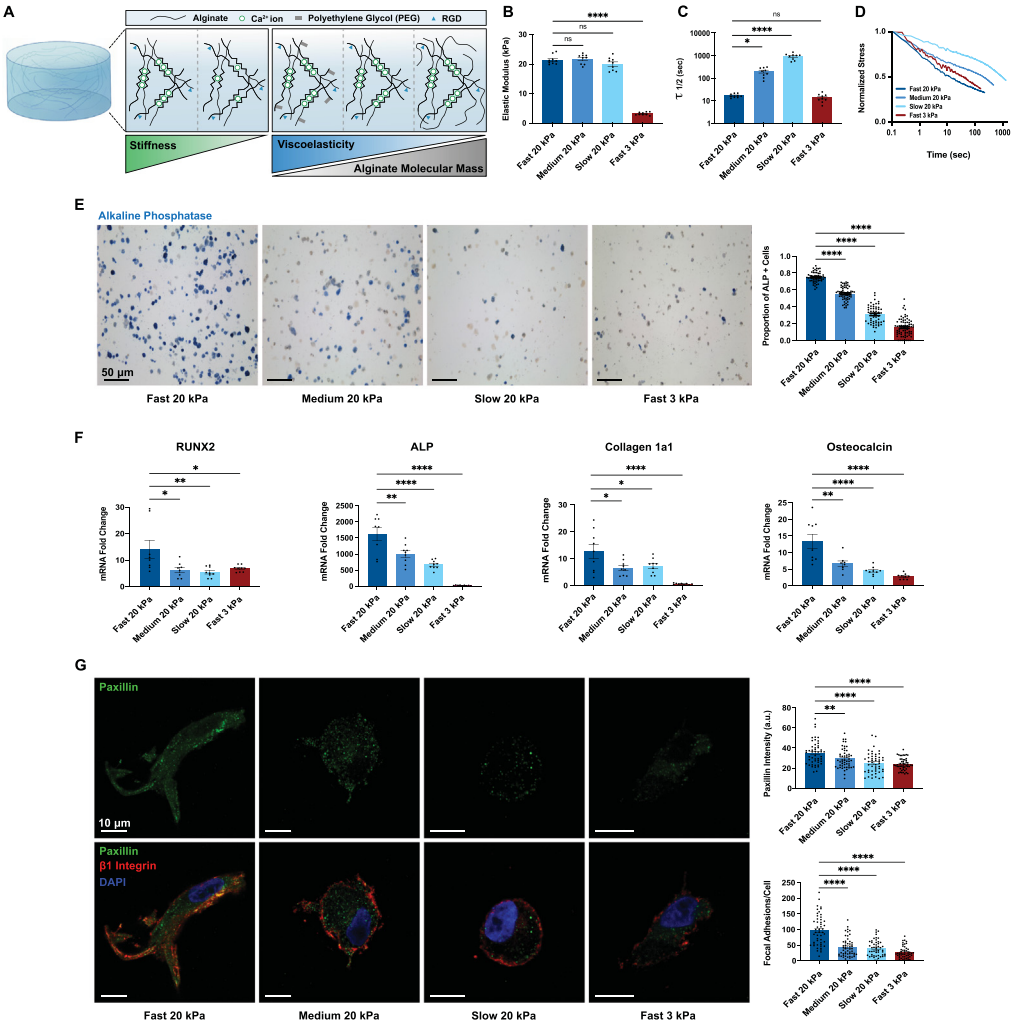

FIGURE 1: Matrix stiffness and stress relaxation direct osteogenesis in 3D. (A) Schematic illustrating the approach to tuning alginate hydrogel mechanical properties. (B) Measurements of the hydrogel elastic modulus one day after crosslinking. (C and D) Quantifications of stress relaxation half-times across hydrogel matrices. (E) Representative images of alkaline phosphatase staining (left) indicate osteogenic differentiation of hBMSCs. Quantification of ALP-positive cells across hydrogel conditions (right). (F) Gene expression data for early osteogenic markers from cells cultured across hydrogel conditions. (G) Representative micrographs of cells cultured across hydrogel conditions stained for paxillin, β1 integrin, and nuclei (left) with quantifications of both paxillin intensity and colocalization of paxillin with β1 integrin (right). Statistical significance was determined by one-way analysis of variance (ANOVA) followed byDunnett's multiple testing correction. $n = 3$ replicates per condition. Error bars represent the S.E.M. * indicates $p < 0.05$, ** $p < 0.01$, *** $p < 0.001$, **** $p < 0.0001$.

adhesion formation are enhanced in fast stress-relaxing matrices (Lou *et al.*, 2018). Furthermore, evidence from the field has demonstrated the necessity of integrin-based signaling to promote mechanically induced osteogenic differentiation (Comisar *et al.*, 2007; Chen and Jacobs, 2013; Chaudhuri *et al.*, 2016; Görlitz *et al.*, 2024; Li *et al.*, 2024a; Wan *et al.*, 2024). In line with these observations, we assessed the extent of focal adhesion formation across our hydrogel conditions by quantifying the colocalization of β1 integrin and paxillin immunofluorescence signals, as well as the total intensity of paxillin fluorescence. Interestingly, cells in stiff, fast-relaxing matrices had significantly more regions of colocalized signals per cell compared with cells in stiff, slower-relaxing or soft, fast-relaxing conditions (Figure 1G). Furthermore, increased focal adhesion marker colocalization coincided with significantly greater cell spreading and decreased cell circularity in the stiff, fast-relaxing matrices, which was evaluated by changes in cell area (Supplemental Figure S1). These results demonstrate an association between stiff, fast-relaxing matrices, enhanced focal adhesion formation, and hBMSC osteogenesis.

Stiff, fast-relaxing matrices promote increased expression of KDM4B and KDM6B

We next sought to investigate how the histone modifiers KDM4B and KDM6B are affected by matrix mechanics. Intriguingly, we found that gene expression of both KDM4B and KDM6B was significantly higher in cells cultured within stiff, fast-relaxing matrices relative to the soft or slow-relaxing hydrogel conditions (Figure 2, A and B). We next aimed to characterize the subcellular localization of KDM4B and KDM6B in different matrix mechanical conditions during osteogenesis by immunofluorescence staining and confocal microscopy. We found that both KDM4B and KDM6B display significantly greater nuclear fluorescence intensity in stiff,

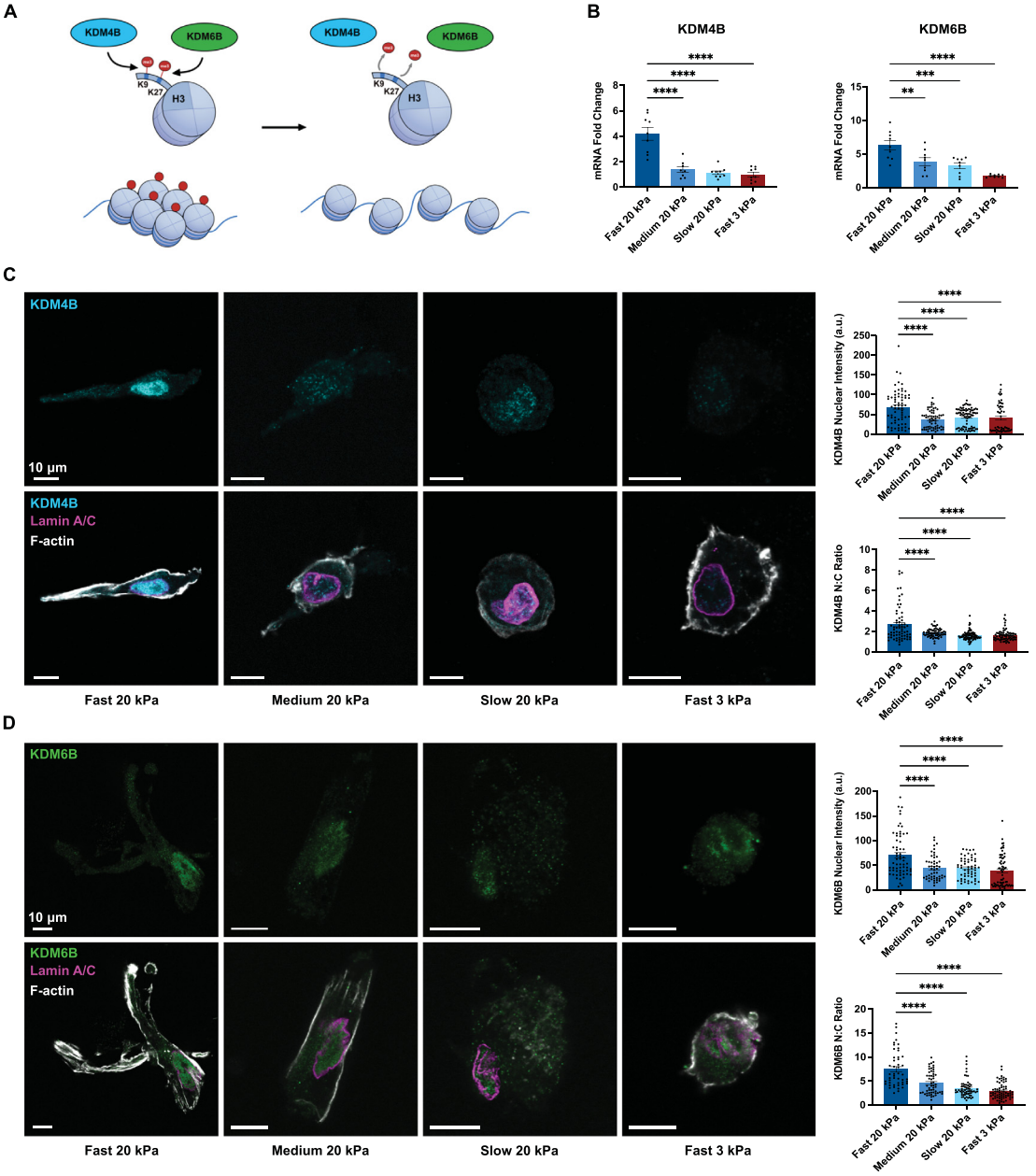

FIGURE 2: Stiff, fast-relaxing matrices promote expression of KDM4B and KDM6B. (A) Schematic illustrating the role of KDM4B and KDM6B during chromatin remodeling. (B) Gene expression of KDM4B and KDM6B between hydrogel conditions after 7 d in culture. (C) Immunofluorescence micrographs of KDM4B (left) and quantifications of KDM4B nuclear intensity and nuclear to cytoplasmic ratio (right). (D) Immunofluorescence micrographs of KDM6B (left) and quantifications of KDM6B nuclear intensity and nuclear to cytoplasmic ratio (right). Statistical significance was determined by one-way analysis of variance (ANOVA) followed by Dunnett's multiple testing correction. $n = 3$ replicates per condition. Error bars represent the S.E.M. ** $p < 0.01$, *** $p < 0.001$, **** $p < 0.0001$.

fast-relaxing matrices compared with all other matrix conditions. Additionally, we found that stiff and fast-relaxing matrices promoted the greatest ratio of nuclear-to-cytoplasmic KDM4B and KDM6B (Figure 2, C and D). These results suggest that KDM4B and KDM6B accumulate within the nucleus in stiff, fast-relaxing matrix conditions to further promote osteogenic gene expression relative to soft or slow-relaxing matrices. Given that KDM4B and KDM6B are histone demethylases that act on trimethylated H3K9 and H3K27 sites, respectively, we assessed the levels of these methylation post-translational modifications from cells across our four matrix conditions. Interestingly, we did not observe any significant differences in the total abundance of H3K9me3 or H3K27me3 after conducting Western blot analysis (Supplemental Figure S2). However, western blotting can only capture global changes in methylation of these respective histone residues, which are potentially acted upon by other histone demethylases as well as methyltransferases. Our findings nonetheless show that matrix viscoelasticity promotes the expression and nuclear localization of KDM4B and KDM6B in an apparent dose-dependent manner.

Stiff, fast-relaxing matrices display reduced H3K9me3 and H3K27me3 levels near transcription start sites

To further investigate how matrix mechanics influence epigenetic regulation during osteogenesis, cleavage under targets and tagmentation (CUT&Tag) profiling of the repressive histone modifications H3K9me3 and H3K27me3 was performed across hydrogel conditions differing in stiffness and stress relaxation. Genome-wide analyses revealed pronounced reductions in both H3K9me3 and H3K27me3 signal proximal to transcription start sites (TSSs) in hBMSCs cultured within stiff, fast-relaxing matrices compared with soft or slow-relaxing conditions (Figure 3, A and B). Additionally, the osteogenic genes RUNX2 and ALP exhibited reduced occupancy of H3K9me3 and H3K27me3, respectively, near their TSSs in stiff, fast-relaxing matrices relative to either soft, fast-relaxing or stiff, slow-relaxing matrix conditions (Figure 3, C and D). To investigate the functional significance of the differential histone methylation profiles on gene expression, we also performed bulk RNA-sequencing on cells cultured in these matrix conditions. Notably, the integration of CUT&Tag and RNA-sequencing datasets demonstrated an inverse relationship between differential gene expression and repressive histone methylation at H3K9 and H3K27 in gene loci associated with osteogenic differentiation (Figure 3, E and F), including vascular endothelial growth factor A (VEGFA), epidermal growth factor receptor (EGFR), and stanniocalcin-1 (STC1). Conversely, many genes involved in bone resorption and matrix degradation processes, such as matrix metalloproteinases (including MMP7, MMP8, and MMP13), displayed the opposite trend of decreased gene expression with correspondingly higher levels of histone repressive marks. Interestingly, these data sets also revealed decreases in expression of certain genes associated with osteogenic differentiation, including BMP4 and IGF1. However, it is not well established how these genes are impacted by matrix stress relaxation.

Principal component analysis of the RNA-seq dataset revealed that cells cultured in stiff, fast-relaxing matrices clustered distinctly from those cultured in soft, fast-relaxing or stiff, slow-relaxing matrices (Supplemental Figure S3). Furthermore, gene ontology pathway analyses showed that upregulated gene sets in stiff matrices were enriched for osteoblast-related signaling pathways, including PI3K-Akt signaling, focal adhesion signaling, EGFR-SMAD1 signaling, as well as regulation of bone mineralization (Figure 3G). Once again, corresponding downregulation of pathways associated with matrix degradation and osteoarthritis was observed in both soft and slow-relaxing matrices. Of note, there were no significantly enriched pathways associated with upregulated genes in fast-relaxing compared with slow-relaxing matrix conditions. These findings demonstrate that viscoelastic matrices are associated with coordinated changes in chromatin state and transcriptional programs that align with enhanced osteogenic differentiation.

Knocking down KDM4B and KDM6B reduces osteogenic differentiation in stiff, fast-relaxing matrices

To interrogate the role of KDM4B and KDM6B during osteogenic lineage commitment in 3D, we transduced hBMSCs with lentiviral shRNA targeting KDM4B or KDM6B before encapsulation in stiff, fast-relaxing matrices. These genetic knockdowns displayed reduced expression of KDM4B or KDM6B relative to the scramble shRNA control group (Figure 4A). Importantly, knocking down the expression of either KDM4B or KDM6B led to significant reductions in ALP-positive cells after one week in culture (Figure 4B). In addition, these knockdowns resulted in significant decreases in gene expression of osteogenic markers, including RUNX2, ALP, Collagen 1a1, and Osteocalcin (Figure 4C), thereby indicating that KDM4B and KDM6B are necessary to regulate early osteogenic lineage commitment. Furthermore, knocking down KDM4B and KDM6B led to marked increases in H3K9me3 and H3K27me3, respectively (Figure 4D), providing further evidence that these histone modifiers are leading to changes in chromatin accessibility during early osteogenic lineage commitment. In addition to knocking down KDM4B and KDM6B, we used pharmacological antagonists to inhibit the catalytic domain of these demethylases. Treatment with inhibitors of KDM4B (ML-324, 10 μM) or KDM6B (GSK-J4, 15 μM) both resulted in significant decreases in osteogenic differentiation compared with the DMSO vehicle control, as assayed by quantification of ALP-positive cells (Supplemental Figure S4A). Additionally, inhibition of KDM4B or KDM6B significantly decreased the expression of the early osteogenic markers RUNX2, ALP, and Collagen 1a1 (Supplemental Figure S4B), which corroborates our observations from genetically perturbing KDM4B and KDM6B expression. Furthermore, we observed a significant decrease in RUNX2 staining intensity in both KDM4B and KDM6B-inhibited groups relative to the vehicle control (Supplemental Figure S4C). Together, these results indicate that KDM4B and KDM6B expression and activity are necessary for hBMSCs to undergo osteogenic differentiation in 3D viscoelastic matrices.

Inhibition of mechanotransduction pathway signaling reduces the expression of KDM4B and KDM6B

Actin cytoskeletal contractility is a well-established mediator of MSC lineage-specific differentiation in response to environmental mechanical cues (Chen and Jacobs, 2013). In particular, Rho-associated kinase (ROCK)-mediated contractility has been shown to positively regulate osteogenic differentiation of MSCs seeded on 2D substrates (McBeath *et al.*, 2004) while exhibiting a concomitant inhibitory effect on adipogenic differentiation (Sordella *et al.*, 2003). Similarly, non-muscle myosin II (NM2) activity has been shown to regulate osteogenic differentiation of MSCs in response to ECM stiffness (Engler *et al.*, 2006). This contractility signaling occurs downstream of actin fiber bundling and focal adhesion kinase (FAK) activation, which are both influenced by integrin receptor clustering (Chaudhuri *et al.*, 2016; Juhl IV *et al.*, 2022). To assess the putative mechanotransduction pathways implicated in driving the expression of KDM4B and KDM6B, we perturbed cellular contractility by inhibiting ROCK (Y-27632, 10 μM), non-muscle myosin II (blebbistatin, 50 μM), or FAK (PF-573228, 10 μM). We observed significant reductions in the number of ALP-positive cells in response to treatment with each of these small-molecule antagonists relative to the vehicle control, demonstrating the impact on hBMSC osteogenesis (Figure 5A). Inhibition of any of the three pathways led to a significant reduction in gene expression of Collagen 1a1, and inhibition of NM2 or FAK resulted in a significant decrease in gene expression of ALP (Figure 5B). Intriguingly, we found no significant differences in RUNX2 gene expression across these inhibitor treatments (Figure 5B). To determine whether KDM4B and KDM6B expression are regulated by these mechanosignaling pathways, we also assessed their expression by qPCR following inhibitor treatment. Expression of KDM4B was significantly decreased across all three mechanotransduction inhibitions (Figure 5B). Inhibition of ROCK or NM2 led to a significant decrease in the expression of KDM6B, though interestingly, there was no significant difference in KDM6B expression upon FAK inhibition compared with the vehicle control.

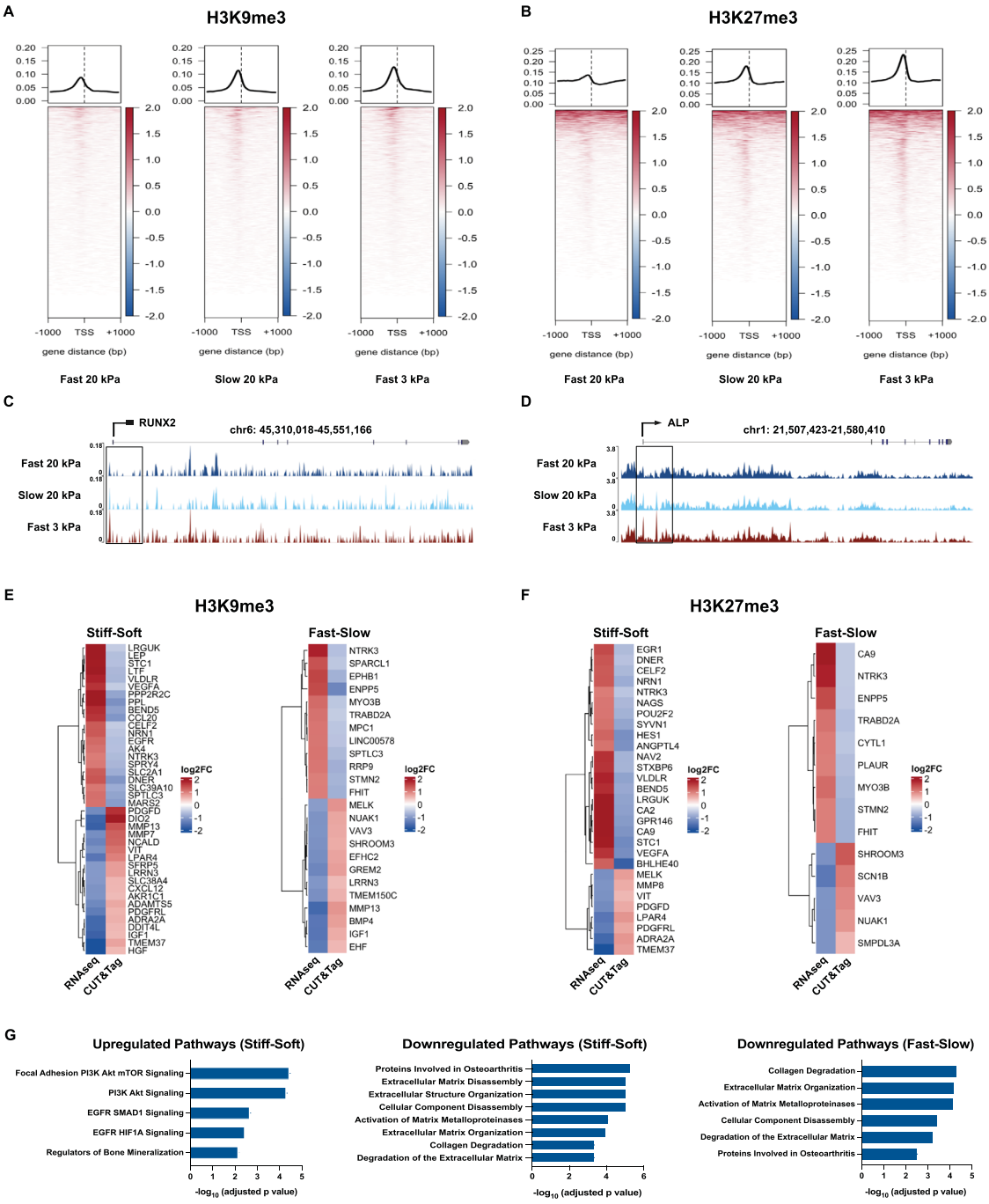

FIGURE 3: Stiff, fast-relaxing matrices show enrichment of osteogenic pathways and reduction in H3K9me3 and H3K27me3 levels. (A) Heat map of genome-wide H3K9me3 and (B) H3K27me3 abundance between matrix conditions 1 kb up and downstream of transcription start sites. (C and D) Integrative genome visualization (IGV) tracks of RUNX2 and ALP genes illustrating reduced H3K9me3 and H3K27me3 abundance in the Fast 20 kPa condition. (E and F) Heat maps of changes in gene expression ($|\text{LogFC}| > 1$, $padj < 0.05$) and histone methylation levels ($|\text{LogFC}| > 0.5$) of cells between matrix conditions. All comparisons are made with respect to the Fast 20 kPa condition. (G) Pathway enrichment analysis for differentially expressed genes ($|\text{LogFC}| > 1$, $padj < 0.05$) in Fast 20 kPa matrices with respect to Slow 20 kPa and Fast 3 kPa conditions.

To further probe FAK-dependent signaling, we inhibited phosphoinositide 3-kinase (PI3K), a canonical downstream effector of FAK (Reif *et al.*, 2003; Zhao and Guan, 2011; Di-Luoffo *et al.*, 2021; Katoh, 2024). Treatment with a highly selective PI3K inhibitor (LY294002, 20 μM) abrogated osteogenic differentiation, as assessed by ALP staining compared with the vehicle control (Supplemental Figure S5). Collectively, these findings indicate that while FAK signaling is required for osteogenesis, regulation of KDM6B expression may occur through parallel, FAK-independent mechanosensitive pathways linked to actomyosin contractility. Therefore, this suggests that numerous orthogonal mechanotransduction pathways converge on osteogenic

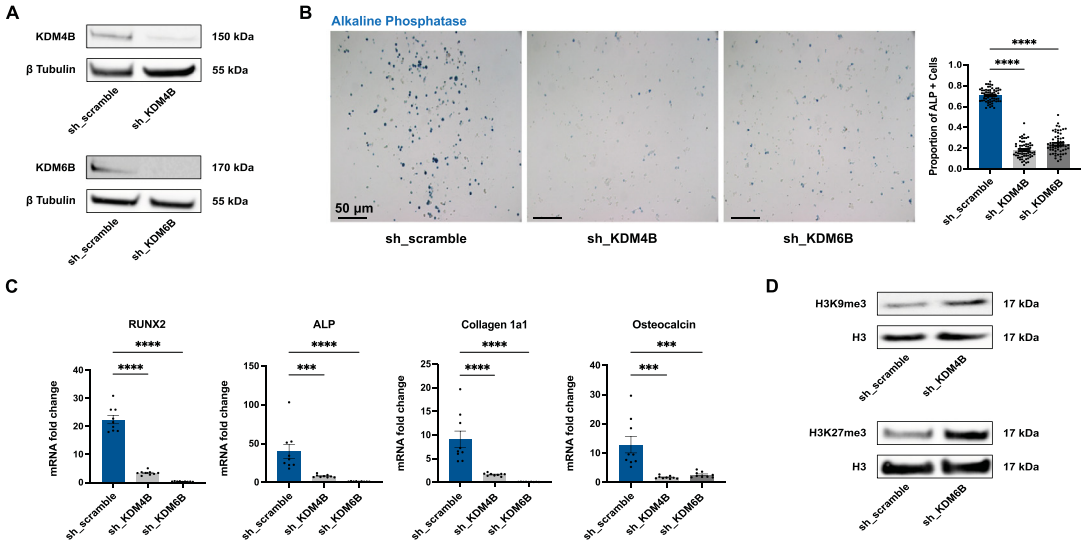

FIGURE 4: Knocking down KDM4B or KDM6B reduces osteogenic differentiation in stiff, fast-relaxing matrices. (A) Western blots of KDM4B (top) and KDM6B (bottom) knockdown samples compared with a non-targeting scramble control. (B) Representative micrographs of stiff, fast-relaxing cryosections with alkaline phosphatase staining between scramble shRNA and KDM-targeted knockdown hBMSC cell lines (left) and quantifications of the proportion of ALP-positive cells (right). (C) Gene expression data for markers of early osteogenic differentiation between scramble and KDM knockdown samples. (D) Western blots of H3K9me3 (top) and H3K27me3 (bottom) from KDM4B and KDM6B knockdown samples, respectively, relative to non-targeting scramble control. Statistical significance was determined by one-way analysis of variance (ANOVA) followed by Dunnett's multiple testing correction. $n = 3$ replicates per condition. Error bars represent the S.E.M. *** indicates $p < 0.001$, **** indicates $p < 0.0001$.

differentiation but differ in their impact on specific epigenetic regulators. Importantly, these results illustrate that KDM4B and KDM6B expression is influenced by perturbations in mechanosignaling.

Given that many cellular force transduction pathways actuate mechanical signaling via cytoskeletal dynamics, we next sought to modulate both actin filament and microtubule stability to investigate their contribution to viscoelasticity-mediated osteogenesis. We used pharmacological disruptors of actin polymerization (cytochalasin D, 1 μM) and actin depolymerization (jasplakinolide, 0.1 μM) to perturb microfilament-based signaling. Additionally, we used a small molecule agonist of microtubule depolymerization (nocodazole, 10 μM) to assess the impact of microtubule-based signaling during early osteogenic differentiation. Compared to the DMSO vehicle control, we observed significant reductions in the number of ALP-positive cells upon treatment with either cytochalasin D or jasplakinolide, whereas nocodazole-treated cells did not show any significant differences in ALP staining relative to the vehicle control (Figure 5C). Additionally, treatment with these drugs led to significant decreases in gene expression for both ALP, Collagen 1a1 (Figure 5D). RUNX2 expression decreased significantly upon treatment with both cytochalasin D and nocodazole, but did not change in expression after treatment with jasplakinolide. Notably, both KDM4B and KDM6B expression significantly decreased upon disruption of actin polymerization and significantly increased in response to actin stabilization (Figure 5D). Microtubule depolymerization significantly decreased the expression of KDM6B, but expression of KDM4B was similar to that of the vehicle control. To that end, this data indicates that early induction of osteogenic gene expression is not necessarily predicated upon the same mechanically actuated signaling patterns, and instead suggests that MSCs utilize numerous, orthogonal force transduction pathways during osteogenic lineage commitment.

Stiff, fast-relaxing matrices increase SMAD 1/5/8 activation and KDM expression.

BMP signaling governs osteogenic differentiation through activation of BMP Type 1 and 2 receptors (Urist, 1997). The cytosolic kinase domains of these receptors induce reciprocal phosphorylation of one another, which then activates these domains to phosphorylate downstream effectors such as SMADs 1/5/8. Upon phosphorylation of SMAD 1/5/8 (pSMAD 1/5/8), these transcription factors translocate to the nucleus and promote expression of osteogenic-related genes (Beederman *et al.*, 2013; Rahman *et al.*, 2015; Wu *et al.*, 2016). Previous research has shown that BMP 4/7 treatment significantly increases KDM4B and KDM6B expression in BMSCs, and that SMAD 1 knockdowns in these same cells led to a decrease in KDM4B and KDM6B expression (Ye *et al.*, 2012). Accordingly, we were curious to investigate the impact of stiffness and stress relaxation on SMAD 1/5/8 activation. We observed the highest abundance of pSMAD 1/5/8 in cells cultured in stiff, fast-relaxing gels via immunofluorescence imaging (Figure 6A). The differences in pSMAD 1/5/8 abundance were significantly greater in stiff and fast-relaxing matrices compared with slower-relaxing or soft matrices.

To investigate the contribution of SMAD 1/5/8 signaling during osteogenic differentiation in stiff, fast-relaxing matrices, we used LDN-193189 (0.1 μM), a small molecule that specifically blocks BMP Type 1 Receptor (BMPR1) phosphorylation of SMAD 1/5/8 (Boergermann *et al.*, 2010). Upon treatment of hBMSCs in stiff, fast-relaxing matrices with LDN-193189 for seven days, we saw a significant decrease in ALP-positive cells relative to the vehicle control (Figure 6B). Inhibition of BMPR1 also led to a significant decrease in gene expression of osteogenic markers RUNX2 and ALP (Figure 6C). Importantly, inhibition of BMPR1 phosphorylation of SMAD 1/5/8 also resulted in significant decreases in gene expression of KDM4B and KDM6B, respectively (Figure 6C). Furthermore, this inhibition also led to a significant decrease in both the

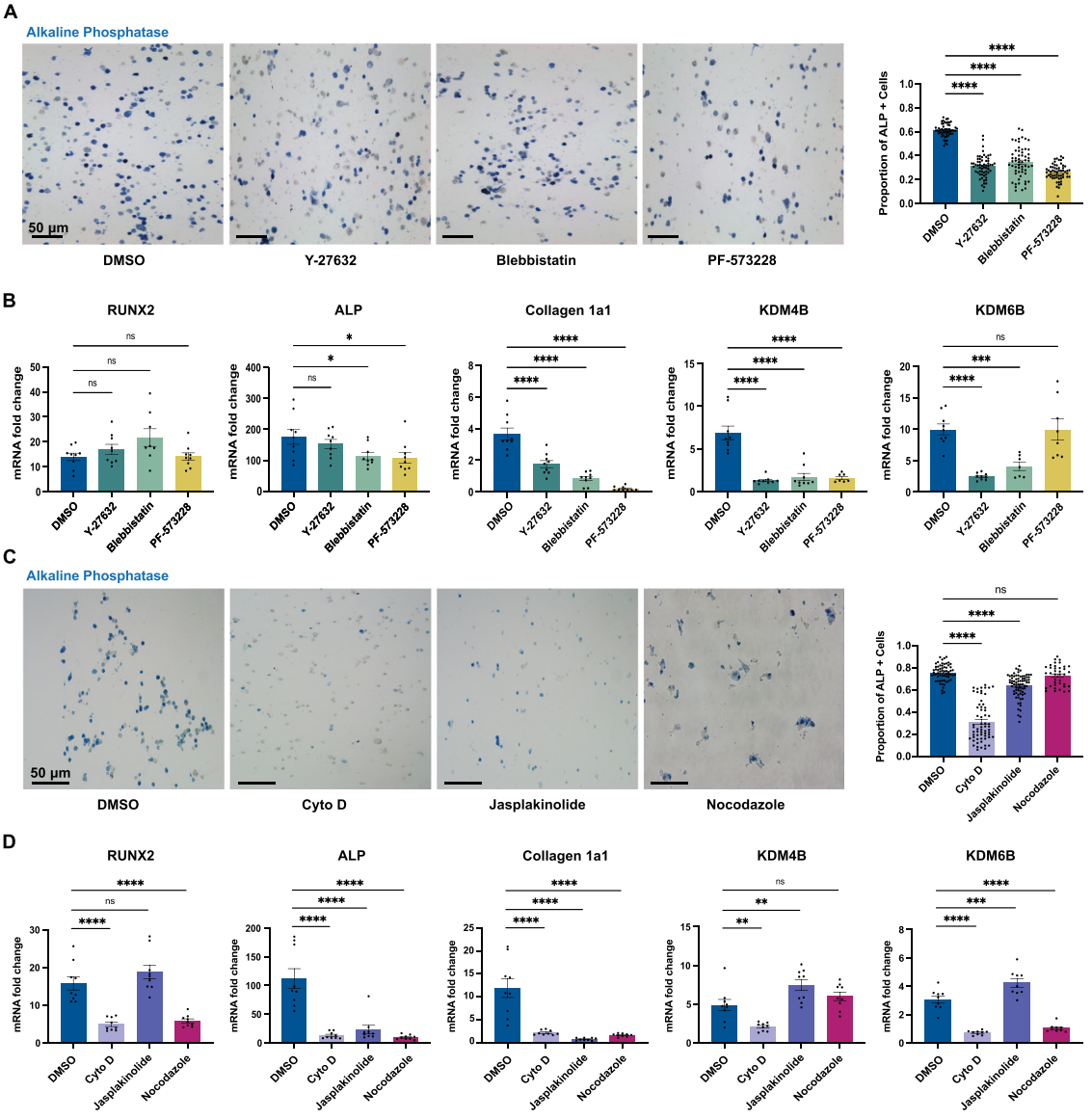

FIGURE 5: Inhibition of mechanotransduction pathways reduces expression of KDM4B and KDM6B. (A) Representative micrographs of ALP-stained stiff, fast-relaxing matrices comparing DMSO-treated and contractility-inhibited conditions (left), and quantifications of ALP-positive cells (right). (B) Gene expression data for osteogenic markers, as well as KDM4B and KDM6B, were compared between DMSO-treated and contractility-inhibited conditions. (C) Representative micrographs of ALP-stained stiff, fast-relaxing matrices comparing DMSO-treated and cytoskeletal modulators conditions (left) with quantifications of ALP-positive cells (right). (D) Gene expression data for osteogenic markers, as well as KDM4B and KDM6B, comparing DMSO-treated and cytoskeletal modulator conditions. Statistical significance was determined by one-way analysis of variance (ANOVA) followed by Dunnett's multiple testing correction. $n = 3$ replicates per condition. Error bars represent the S.E.M. * indicates $p < 0.05$, ** $p < 0.01$, *** $p < 0.001$, **** $p < 0.0001$.

nuclear localization and abundance of KDM4B and KDM6B relative to the vehicle control (Figure 6, D–E). Additionally, we assessed the levels of pSMAD 1/5/8 in cells where mechanotransduction and cytoskeletal signaling pathways were inhibited. Here, we identified that inhibiting NM2 and FAK led to significant decreases in pSMAD 1/5/8 signal relative to the vehicle control (Supplemental Figure S6). However, inhibition of ROCK did not lead to any statistical differences in pSMAD 1/5/8 intensity. Upon perturbing cytoskeletal dynamics, inhibition of actin filament polymerization with cytochalasin D significantly decreased pSMAD 1/5/8 signal, while inhibition of actin filament depolymerization resulted in significantly increased pSMAD 1/5/8 signal compared with the vehicle control. However, treatment with nocodazole did not lead to any significant changes in pSMAD 1/5/8 signal intensity, suggesting that pSMAD 1/5/8 signaling is potentially modulated by actin filament dynamics rather than through microtubule signaling. Collectively, these results illustrate a linkage between BMP signaling, mechanotransduction, and the expression of KDM4B and KDM6B, providing insight into how matrix mechanical cues influence BMP receptor activity during osteogenic lineage commitment.

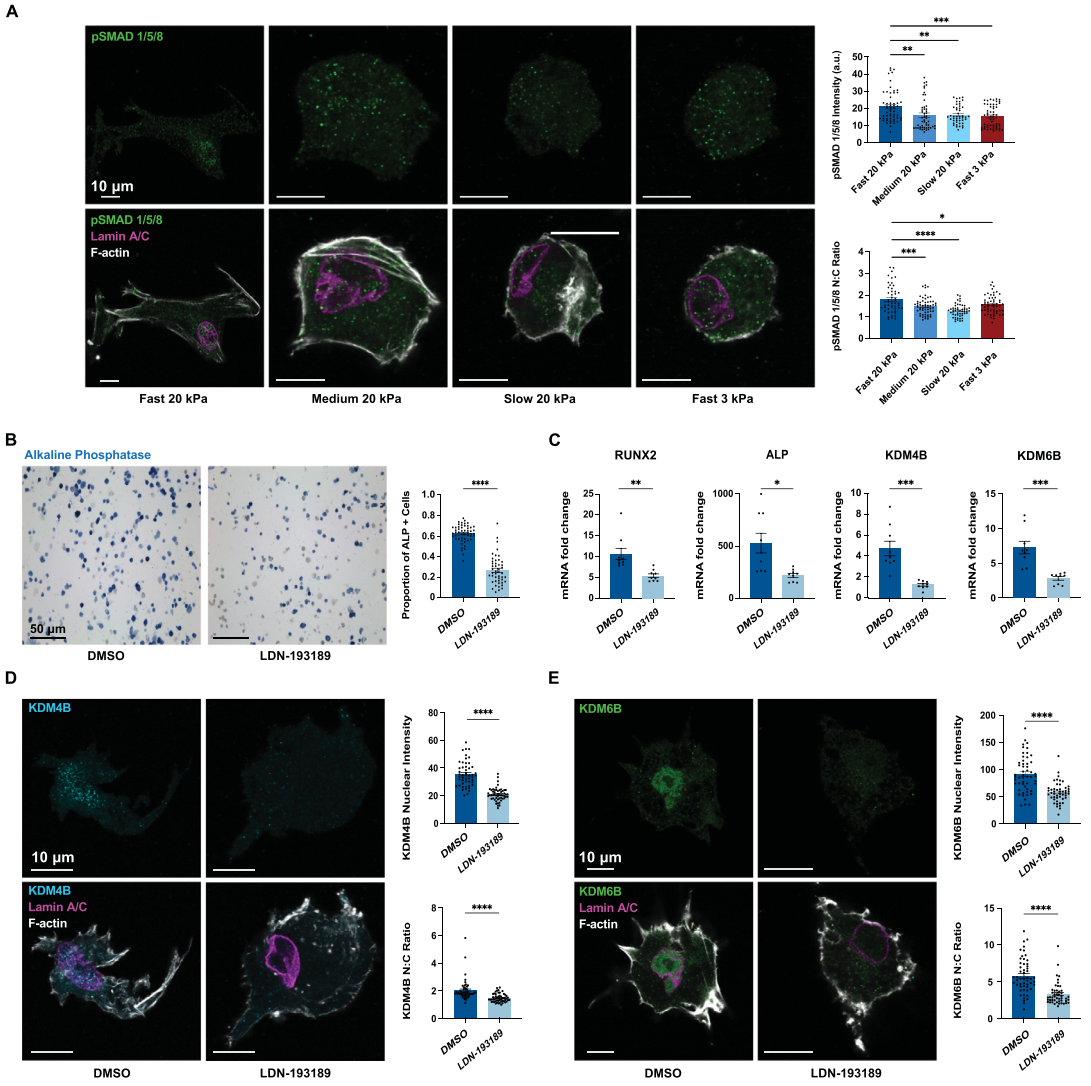

FIGURE 6: Viscoelasticity increases BMP-SMAD pathway signaling and regulates expression of KDM4B and KDM6B. (A) Representative micrographs of cells cultured across matrix conditions stained for phospho-SMAD 1/5/8, lamin A/C, and F-actin (left) with quantifications of signal intensity and nuclear to cytoplasmic ratio (right). (B) Alkaline phosphatase staining of cells in stiff, fast-relaxing matrices comparing DMSO-treated and BMPR1-inhibited media conditions (left) with quantification of ALP-positive cell proportions. (C) Gene expression quantifications of DMSO-treated and BMPR1-inhibited conditions. (D and E) Representative micrographs of cells stained for KDM4B, KDM6B, lamin A/C, and F-actin between DMSO-treated and BMPR1-inhibited conditions, with quantifications of nuclear to cytoplasmic ratio and nuclear intensity. For panel A, statistical significance was determined by one-way analysis of variance (ANOVA) followed by Dunnett's multiple testing correction. For panels B–E, statistical significance was determined by unpaired *t* tests with Welch's correction. $n = 3$ replicates per condition. Error bars represent the S.E.M. * indicates $p < 0.05$, ** $p < 0.01$, *** $p < 0.001$, **** $p < 0.0001$.

DISCUSSION

In this study, we investigated the mechanobiological regulation of histone demethylases KDM4B and KDM6B during early osteogenic differentiation in human BMSCs. We observed that matrix stiffness and stress relaxation rate modulate the expression and nuclear localization of both KDM4B and KDM6B, and that inhibition of several mechanotransduction pathways decreases the expression of these demethylases. Our findings represent one of the first investigations into how both histone demethylation and SMAD 1/5/8 activation are influenced by matrix viscoelasticity, thus providing new insight into how BMSCs integrate ECM mechanical cues to coordinate lineage specification. To that end, our results also contribute to an emerging field investigating how matrix mechanics shape cell fate outcomes through epigenetic regulation by histone-modifying enzymes.

Recent findings in the field of mechanobiology have illustrated an interplay between mechanotransduction signaling and epigenetic remodeling during phenotypic transitions across a variety of mesenchymal-derived cell types in direct response to microenvironmental cues (Downing *et al.*, 2013; Heo *et al.*, 2015, 2023; Roy *et al.*, 2018, 2020; Wu *et al.*, 2025). In the context of disease onset, such as gastric and mammary tumorigenicity, changes in ECM mechanics have been linked to aberrations in gene expression specifically through changes in DNA methylation, chromatin accessibility,

and HDAC3 and HDAC8 activity (Stowers *et al.*, 2019; Jang *et al.*, 2021). Interestingly, hallmarks of osteogenic differentiation in BMSCs have been shown to correlate with both changes in expression of histone deacetylases and associated histone acetylation in response to stiff substrates (Killaars *et al.*, 2019, 2020). However, the impact of stress relaxation on epigenomic changes during stem cell differentiation has not been studied to date. Our findings contribute to the burgeoning effort to understand how ECM mechanical properties drive changes in cell fate through the activity of epigenetic signaling pathways.

Our results corroborate previous reports that KDM4B and KDM6B are essential for the induction of osteogenesis and that loss of either KDM4B or KDM6B significantly reduces expression of early osteogenic markers (Ye *et al.*, 2012; Deng *et al.*, 2022; Jin *et al.*, 2022; Ying *et al.*, 2024). In line with these observations, our findings that either knocking down expression or inhibiting catalytic activity of KDM4B and KDM6B lead to reduced expression of essential osteogenic markers in viscoelastic matrices provide new evidence for how biophysical cues mediate epigenetic regulatory events. Previous findings have identified that KDM4B removes repressive methylation marks from the promoter of RUNX2, a master regulator of osteogenic differentiation, to facilitate its transcription and establish osteogenic lineage commitment (Kang *et al.*, 2022). Our CUT&Tag results indicate that the RUNX2 gene undergoes coordinated demethylation near its TSS in response to differential ECM viscoelasticity, providing further mechanistic detail for mechanically induced osteogenic differentiation. Similarly, KDM6B depletion has been shown to significantly reduce ALP activity and associated mineral deposition (Xu *et al.*, 2013). To that effect, our CUT&Tag results indicate that the ALP gene exhibits decreased H3K27me3 enrichment near its TSS in stiff, fast-relaxing matrices relative to soft or slower-relaxing matrix conditions, suggesting that coordinated modulation of repressive histone modifications occurs between matrix viscoelastic conditions. Moreover, these observations indicate that ECM mechanics are indeed associated with distinct chromatin states, particularly at regulatory regions linked to transcriptional control during osteogenic differentiation. Thus, our work contributes to a growing body of literature showing numerous, orthogonal signaling pathways that promote osteogenesis, including via epigenomic remodeling by histone modifiers such as KDM4B and KDM6B.

CUT&Tag profiling illustrates that hBMSCs cultured in stiff, fast-relaxing matrices display a pronounced reduction in global H3K9me3 and H3K27me3 repressive marks proximal to TSSs, which is consistent with a transcriptionally permissive chromatin state. This coordinated demethylation was also accompanied by increased expression of osteogenesis-associated genes such as VEGFA, EGFR, and STC1. Integration of CUT&Tag and RNA-seq data revealed a clear inverse relationship between repressive histone occupancy near TSSs and gene expression, which suggests a mode of spatially localized chromatin remodeling in response to mechanosignaling. In contrast, genes associated with matrix degradation and bone resorption retained higher levels of repressive histone methylation and were transcriptionally downregulated under these conditions. Together, these findings suggest that stiff, fast-relaxing matrices promote osteogenic differentiation through a selective reduction in repressive histone modifications at promoter regions, thereby reinforcing osteoblast lineage-specific transcriptional programs.

ECM mechanics are well-established to regulate osteogenesis (Rath *et al.*, 2011; Hwang *et al.*, 2015; Chaudhuri *et al.*, 2016; Darnell *et al.*, 2018a; Lee *et al.*, 2019; Killaars *et al.*, 2020; Li *et al.*, 2024b), and significant work in the field of mechanobiology has demonstrated that mechanotransduction pathways are essential for osteogenic differentiation. Our use of pharmacological inhibitors targeting downstream effectors of integrin signaling, including ROCK, NM2, and FAK, provides novel evidence that KDM4B and KDM6B are sensitive to various force transduction modalities. While expression of both KDM4B and KDM6 B was significantly decreased upon inhibiting ROCK and NM2, RUNX2 expression did not change significantly in response to these inhibitors. MSCs have long been understood to differentiate based on actomyosin-driven signaling (Engler *et al.*, 2006), but prior work has also shown that RUNX2 mRNA levels do not change upon ROCK inhibition (Prowse *et al.*, 2013) and that numerous upstream regulatory processes may govern its expression beyond cytoskeletal contractility (Franceschi *et al.*, 2003). Reports have also shown that FAK inhibition significantly reduces both ALP and Collagen 1a1 expression in BMSCs cultured in 2D (Rajshankar *et al.*, 2017; Gunn *et al.*, 2022), which corroborates our observations of this inhibition in stiff, fast-relaxing 3D matrices. While we observed a significant decrease in KDM4B expression upon inhibiting FAK, this inhibition did not lead to a significant difference in KDM6B mRNA levels. Additionally, our findings that the prevention of either actin or microtubule polymerization decreases the expression of KDM6B, as well as RUNX2, ALP, and Collagen 1a1, reinforce that mechanotransduction-mediated osteogenesis relies on cytoskeletal force transduction for coordinated biophysical signal integration (Xu *et al.*, 2017; Sun *et al.*, 2021; Li *et al.*). Conversely, our results show that actin filament stabilization increases the expression of both KDM4B and KDM6B, which implies that force transduction pathways may promote the expression of histone modifiers, which is an important avenue for future investigation. Interestingly, treatment with the microtubule disassembly agonist nocodazole did not significantly alter KDM4B expression relative to the vehicle control. Therefore, BMSCs may potentially utilize numerous orthogonal pathways to upregulate KDM4B and KDM6B during mechanically induced osteogenesis.

Smad 1/5/8 activation is known to regulate osteogenesis of BMSCs (Wu *et al.*, 2016). Recent findings have suggested that stiff substrates augment osteogenesis by potentiating the activity of the BMP-SMAD 1/5/8 signaling axis (Görlitz *et al.*, 2024). Additionally, prior work has identified a reciprocal association between integrin signaling and BMPR activity resulting in increased SMAD 1/5 activation (Zhou *et al.*, 2013). Accordingly, our results showing that actin filament stabilization led to increased pSMAD 1/5/8 signal in viscoelastic matrices support this association between cell-ECM signaling and SMAD pathway activity. Additionally, inhibition of actomyosin contractility has been shown to decrease the response of BMSCs to BMP signaling in 3D culture (Rath *et al.*, 2011; Li *et al.*, 2024b), which is corroborated by our findings that treatment with both blebbistatin and cytochalasin D led to significantly decreased phosphorylation of SMAD 1/5/8 in stiff, fast-relaxing matrices. These results indicate that both stiffness and stress relaxation exert an effect on SMAD 1/5/8 signaling, and that this pathway regulates the expression of histone modifiers KDM4B and KDM6B, as well as canonical osteogenic markers RUNX2 and ALP. A recent report has also shown that collagen alignment upregulates SMAD 1/5/8 signaling in MSCs in the absence of BMP ligands onto cells (Heo *et al.*, 2025), where the alignment of collagen fibers within the ECM promotes cell spreading and mechanosignaling. Despite the lack of collagen or any fibrillar ECM component, we also found similar significant increases in cell spreading and focal adhesion marker abundance in stiff, viscoelastic matrices. Additionally,

another report showed that disruptors of either actin polymerization or myosin ATPase activity negatively regulated SMAD 1/5/8 phosphorylation and precluded robust osteogenic differentiation (Xu *et al.*, 2017), which is also in line with our observations in 3D viscoelastic matrices. These results indicate a potential overlap in canonical BMP signaling with biophysical elements of the cellular microenvironment, and that BMP-regulation of osteogenesis is predicated, in part, on cell-ECM interactions. This convergence of both biochemical and mechanical regulation of SMAD 1/5/8 activity serves as a promising target of future investigations exploring mechanisms linking mechanotransduction to changes in chromatin accessibility. An improved understanding of these signaling pathways will therefore inform the design of biomaterial platforms utilized for bone regeneration in the context of critical wound healing and age-related bone loss.

In conclusion, our work shows a novel mechanoresponsive role for KDM4B and KDM6B in regulating BMSC osteogenesis. Specifically, we found that the expression and nuclear abundance of KDM4B and KDM6B are enhanced in stiff and fast-relaxing matrices during osteogenesis, and that reductions occur in H3K9me3 and H3K27me3 enrichment at key osteogenic loci in response to differential matrix viscoelasticity. These results illustrate that both ECM stiffness and stress relaxation regulate hBMSC fate via activation of mechanosignaling pathways and, further, that SMAD 1/5/8 phosphorylation is upregulated in stiff, fast-relaxing matrices. Our work provides insight into how ECM mechanics are linked to epigenetic regulation and how the delineation of these signaling pathways can be leveraged to guide stem cell fate for applications in both disease modeling and regenerative medicine.

MATERIALS AND METHODS

Request a protocol through *Bio-protocol*

Hydrogel preparation

Pronova VLVG and LF 20/40 alginate were purchased from NovaMatrix and prepared as previously described (Rowley *et al.*, 1999; Chaudhuri *et al.*, 2016). Briefly, RGD-modified alginate was prepared by conjugating the oligopeptide GGGGRGDSP (Peptide 2.0) to the alginate polymers using carbodiimide chemistry at a final concentration of 1500 μM RGD in 2% wt/vol alginate hydrogels. Alginate was then dialyzed against deionized water for 2–3 days (molecular weight cutoff of 10 kDa), treated with activated charcoal, sterile filtered, lyophilized, and then reconstituted in serum-free Dulbecco's Modified Eagle Medium (DMEM, Life Technologies). Polyethylene glycol (PEG)-alginate was prepared by coupling PEG-amine (5 kDa, Laysan Bio) to VLVG alginate using carbodiimide chemistry and purified with a similar procedure to the RGD coupling.

Mechanical characterization

Rheology measurements were conducted using a stress-controlled Anton Paar MCR 502 rheometer. Hydrogels were cast between silanized glass plates with a 2 mm spacer, biopsy punched into 8 mm diameter discs, and allowed to swell in DMEM overnight. The storage modulus (G') and loss modulus (G'') of alginate gels were measured at a frequency of 1 Hz with 0.1% applied shear strain. The complex modulus (G*) was measured and used to calculate the elastic modulus (E), as shown below. The Poisson's ratio (υ) was assumed to be 0.5 (Charbonier *et al.*, 2021).

$$G^* = \left(G'^2 + G''^2\right)^{1/2}$$

$$E = 2G^*(1+\nu)$$

Stress relaxation tests were conducted using a constant strain of 15%. The time required for each gel sample to reach half of the maximum stress was used to determine the stress relaxation time ($\tau_{1/2}$) for each gel condition across three independent replicates. Gel recipes are detailed in Supplemental Table S1.

Cell Culture

Primary human BMSCs (hBMSCs) were obtained from Millipore Sigma (SCC034) and cultured according to established protocols (Huebsch *et al.*, 2010; Darnell *et al.*, 2017). Cells were expanded in low-glucose DMEM in the presence of 20% FBS (ThermoFisher) and 1% Pen/Strep (Life Technologies) and maintained below 80% confluency.

Cell Encapsulation and Osteogenic Differentiation

hBMSCs used in this study were expanded up to passage 4 before encapsulation in hydrogel matrices. Cells were washed twice with Dulbecco's phosphate-buffered saline (DPBS) before trypsinization in 0.25% trypsin/EDTA (Life Technologies). Cells were then suspended in DMEM and mixed with alginate. The alginate-cell solution was mixed with $CaSO_4$ and immediately cast between two glass plates. Upon gelation, gels were punched using 8 mm biopsy punches and cultured in OsteoMAX differentiation media (Millipore Sigma, SCM121) for 7 d with media changes occurring every 2 days.

Immunofluorescence Staining

Encapsulated cells were fixed in 4% paraformaldehyde (PFA) for 45 min and then washed three times in DPBS with Ca^{2+}/Mg^{2+} for 15 min each. The hydrogels were then dehydrated in a 30% sucrose solution in DPBS overnight and then incubated in a 1:1 mixture of 30% sucrose and OCT solution (ThermoFisher, 23730571) before freezing on dry ice. Frozen hydrogel samples were cryosectioned into 40 μm-thick slices and adhered to polylysine-coated slides for subsequent staining procedures. Slides were blocked with a solution of 10% goat serum (ThermoFisher), 1% bovine serum albumin (Sigma), 0.1% Triton X-100 (Sigma), and 0.3 M glycine (Sigma) for 1 h at room temperature. Primary antibodies were diluted in the blocking solution and incubated at 4°C overnight. The slides were then washed three times in DPBS for 5 min each before being incubated with Alexa Fluor 488, 555, or 647 secondary antibodies in blocking solution for 1 h at room temperature. Alexa Fluor 488 or 647–phalloidin (1:100 dilution, ThermoFisher) and 4′,6-diamidino-2-phenylindole (DAPI, 1 μg/ml, ThermoFisher) were also diluted in the blocking solution and simultaneously incubated with secondary antibodies for 1 h. The slides were then washed three times for 5 min in DPBS, and coverslips were applied with Prolong Gold antifade reagent (ThermoFisher, P36930). Antibodies used in this study include Integrin β1 (ThermoFisher, 14-0299-82), Paxillin (Cell Signaling Technologies, 50195S), KDM4B (Cell Signaling Technologies, 8639), KDM6B (Abcam, ab169197), RUNX2 (Cell Signaling Technologies, 12556S), Lamin A/C (Cell Signaling Technologies, 4777S), and phospho-SMAD 1/5/8 (Cell Signaling Technologies, 13820). Slides were imaged on a Leica SP8 laser scanning confocal microscope with a 63x objective.

ALP Staining

ALP was stained using Fast Blue BB Salt (Millipore Sigma, F3378) and naphthol-AS-MX phosphate (Millipore Sigma, N4875) at a working concentration of 500 μg/ml each in an alkaline buffer

(100 mM Tris-HCl, 100 mM NaCl, 0.1% Tween-20, 50 mM MgCl2, pH = 8.2). Poly lysine-coated slides with affixed cryosections were washed three times in DPBS, equilibrated in alkaline buffer for 15 min, then incubated in FastBlue working solution for 60 min at room temperature. The slides were then washed for 15 min in alkaline buffer, followed by three washes in DPBS for 5 min each and mounted using Prolong Gold antifade reagent. Slides were imaged using an Olympus BX60 Upright microscope using a color camera and a 10× objective. The number of ALP-positive cells was enumerated and then divided by the total number of cells in each field of view to determine the total proportion of ALP-positive cells.

Image Analysis

FIJI (NIH) was used for image analysis to quantify cell area, circularity, localization, and intensity of the selected markers used in this study. The plugin Ilastik was used to analyze confocal microscopy images and generate subcellular region-specific ROIs that assign labels to pixels based on their unique features and user annotations. The generated ROIs were imported into ImageJ, where a custom macro was used to threshold, analyze, and create a mask of defined cell regions. The quality of the mask was manually verified before defining a Region of Interest (ROI) and measuring the fluorescent intensity.

To determine the nuclear-to-cytoplasmic signal ratio, masks were generated for the cell nucleus (lamin A/C) and cell outline (phalloidin). The nuclear mask was subtracted from the cell outline mask to generate an ROI for the cytoplasm, then both the cytoplasm and nuclear ROI were measured for the protein channel of interest. The mean fluorescence intensity in each ROI was calculated by dividing the total fluorescence intensity by the number of pixels measured.

Focal adhesions were identified by the colocalization of paxillin and integrin $\beta 1$. To assess this, the same Ilastik pipeline was used to generate cell outline masks based on F-actin staining. The ImageJ plugin *ComDet* was then used to quantify the degree of colocalization within each cell ROI, using an average particle size of 8 pixels, a maximum distance of 6 pixels between the centers of colocalized spots, and an intensity threshold set to 20 standard deviations above the mean for both paxillin and integrin $\beta 1$ channels. Additionally, the mean fluorescence intensity of paxillin was measured within each cell ROI.

Quantitative Real-Time PCR

Cells were extracted from hydrogels by chelation of calcium ions using 50 mM EDTA in DPBS. Cell pellets were washed twice with DPBS to remove residual EDTA. Cells were then lysed with Trizol (Life Technologies, 10296028) and RNA was extracted according to the manufacturer's instructions (Epoch Life Sciences, 1660250). Purified RNA was then reverse-transcribed into complementary DNA (cDNA) using a High-Capacity cDNA Reverse Transcription Kit (Applied Biosystems, 4368814). Here, 10 ng of cDNA was used for each quantitative real-time PCR (qRT-PCR) reaction, performed in triplicate for each biological replicate. SYBR Green PCR Master Mix (ThermoFisher, A25742) was used for amplification of target sequences on a CFX96 Touch Real Time Detection System (Bio-Rad). Relative gene expression was calculated using the $2^{-\Delta\Delta Ct}$ method (Livak and Schmittgen, 2001). The primer sequences are detailed in Supplemental Table S2.

CUT&Tag Sequencing and Analysis

CUT&Tag was performed essentially as described by Kaya-Okur et al (Kaya-Okur *et al.*, 2019) using the Active Motif CUT&Tag-IT kit (Active Motif, 53176), with slight modifications (Kaya-Okur *et al.*, 2020). Briefly, 100,000 cells were pelleted (600 × g, 5 min) and resuspended in 1 ml wash buffer supplemented with protease inhibitors. Concanavalin A beads were activated in 1 × binding buffer and incubated with the cells for 10 min at room temperature. Bead-bound cells were resuspended in 50 µl antibody buffer containing 0.05% digitonin, protease inhibitor, and primary antibodies against H3K27me3 (Cell Signaling, 9733S) and H3K9me3 (Abcam, ab1220), followed by overnight incubation at 4°C. Cells were washed in Dig-Wash buffer (0.05% digitonin, protease inhibitor) and incubated for 1 h at room temperature with anti-rabbit secondary antibody (1:100). After two washes, pA-Tn5 transposome (1:100 in Dig-300 buffer containing 0.01% digitonin and protease inhibitor) was added and incubated for 1 h at room temperature. Following two washes in Dig-300, tagmentation was performed in 125 µl tagmentation buffer (0.01% digitonin, protease inhibitor) for 1 h at 37°C. Tagmentation was stopped by two washes with 10 mM TAPS buffer containing 0.2 mM EDTA, after which cells were resuspended in 5 µl releasing buffer (0.1% SDS) and incubated at 55°C for 1 h. Samples were neutralized with 15 µl neutralization buffer (0.67% Triton X-100), and sequencing libraries were generated using Illumina i5/i7 indexed primers and NEB 2 × PCR master mix (NEB, M0541L).

Library fragment-size distributions were assessed using an Agilent Bioanalyzer 2100, and DNA concentrations were measured by Qubit fluorometry. Libraries were sequenced on an Illumina NovaSeq X platform using 150-bp paired-end reads. Paired-end reads were aligned to the human hg38 reference genome using Bowtie2 (v2.3.5). PCR duplicates were removed using Picard, and normalized genome coverage tracks were generated using bamCoverage (deepTools). Tracks were visualized with pyGenomeTracks. Transcription start site (TSS) enrichment was calculated using computeMatrix with ±1 kb windows centered on TSS, and heatmaps were generated with deepTools. Peak annotation and genomic distribution analyses, including pie charts, were performed using HOMER. Primary peak summits were identified using MACS2 with a false-discovery rate cutoff of $q < 0.01$. Peaks overlapping between biological replicates were merged, and summit positions were recentered and uniformly extended by ± 250 bp to generate fixed-width peak regions for downstream quantification. A consensus peak set and corresponding read counts were obtained using DiffBind, which assembled the merged peak set across samples and quantified fragment counts within each region.

RNA Sequencing

Cells were extracted from alginate hydrogels by chelation of calcium ions using 50 mM EDTA in DPBS. Cell pellets were washed twice with DPBS to remove residual EDTA. Cells were then lysed with Trizol (Life Technologies, 10296028) and RNA was extracted according to the manufacturer's instructions (Epoch Life Sciences, 1660250). Bulk mRNA sequencing libraries were generated following the Cel-Seq2 protocol as previously described (Hashimshony *et al.*, 2016). In brief, 10 ng of isolated RNA was converted to cDNA using a Cel-Seq2–specific reverse transcription primer in the presence of 0.1 M DTT, dNTPs (New England Biolabs, N0447L), and SuperScript II reverse transcriptase (Invitrogen, 18064014). Double-stranded cDNA synthesis was subsequently carried out using RNase H (ThermoFisher Scientific, EN0202), *E. coli* DNA polymerase I (Invitrogen, 18010025), *E. coli* DNA ligase (Invitrogen, 18052-019), and the corresponding second-strand synthesis buffer (Invitrogen, 18052-019). Following cDNA purification with magnetic DNA beads (AMPure, A63882), amplified RNA was

generated via in vitro transcription using the MEGAscript T7 transcription system (Invitrogen, A57622). The resulting single-stranded aRNA was treated with ExoSAP-IT PCR cleanup reagent (ThermoFisher, 78200) before controlled fragmentation in a buffer composed of 200 mM Tris-acetate (pH 8.1), 500 mM potassium acetate, and 150 mM magnesium acetate. Fragmentation was stopped using EDTA (500 mM). Fragmented aRNA was subsequently purified using RNA-specific magnetic beads (AMPure, A63987). Purified aRNA was reverse transcribed using random hexamer primers, followed by cDNA amplification with an RNA PCR primer (RPI), a sample-specific indexed Illumina primer, and a PCR master mix (New England Biolabs, M0541S). Final libraries were cleaned using bead-based purification and assessed for quality and size distribution with an Agilent Bioanalyzer. Sequencing was performed on Illumina X platforms. Resulting sequencing reads were aligned to the human reference genome (hg19/GRCh37). Differential gene expression analysis was conducted in R using the DESeq2 package, applying a log2 fold-change threshold of $\geq$1 and an adjusted *p*-value cutoff of 0.05. Pathway enrichment analysis was performed using enrichR (Kuleshov *et al.*, 2016).

RNA Interference

Single-stranded shRNA oligos were obtained from Integrated DNA Technologies (IDT) and cloned into the pLKO.1 lentiviral transfer vector (Addgene, 10878). Clone IDs for these sequences were TRCN0000018016 (KDM4B) and TRCN0000236677 (KDM6B), respectively, with a scramble shRNA plasmid (Addgene, 1864) used as a negative control. Upon validation of cloned constructs using Sanger sequencing, lentiviral particles were produced by co-transfecting transfer, packaging (Addgene, 12260), and envelope (Addgene 12259) plasmids into 293T cells using 1 mg/ml PEI transfection reagent (Kyfora Bio, 24765). Lentivirus-containing media were harvested at 48 h post-transfection, concentrated using Lenti-X Concentrator (VWR, 101739-066), and filtered through a 0.45 µm filter. P2 hMSCs were cultured to 70% confluence before being infected with viral supernatant at a 1:10 ratio in culture media containing no antibiotics and 100 µg/ml protamine sulfate (Lin *et al.*, 2012). Media was then replaced after 24 h and was supplemented with 1 mg/ml puromycin during every subsequent media change. Experiments were conducted using P4 hMSCs selected by puromycin throughout cell encapsulations.

Western blotting

Cells were extracted from hydrogels by chelation of calcium ions using 50 mM EDTA in DPBS. Once pelleted, cells were washed twice with DPBS to remove any residual EDTA. Cells were then lysed via sonication for 30 seconds in RIPA buffer (ThermoFisher, 89901) along with protease and phosphatase inhibitor cocktail (ThermoFisher, 78440). Protein lysates were centrifuged to pellet cell debris, and the supernatant was collected and used for further analysis. Protein samples were separated using SDS–PAGE and transferred to nitrocellulose membranes. Membranes were blocked in Tris-buffered saline (TBS) with 5% wt/vol nonfat milk and incubated with primary antibodies for KDM4B (Cell Signaling, 8639), KDM6B (Abcam, ab169197), β-Tubulin (Cell Signaling, D3U1W), H3K9me3 (Cell Signaling, D4W1U), H3K27me3 (Cell Signaling, C36B11), and H3 (ThermoFisher, 39763) at 4°C overnight. Membranes were then washed with TBS with 0.05% Tween-20 (TBST) and incubated with Alexa Fluor-conjugated IgG secondary antibodies (ThermoFisher) or IRDye 800CW anti-mouse (LICOR, 925-32212) and anti-rabbit (Cell Signaling, 5151P) secondary antibodies for 1 h. Protein bands were imaged on a ChemiDoc system (Bio-Rad).

Pharmacological Inhibition

For inhibition experiments, small molecule inhibitors of KDM4B (ML-324, 10 µM) and KDM6B (GSK-J4, 15 µM) were added to the differentiation media for culture over 7 days. For inhibition of mechanotransduction signaling, small molecule antagonists of ROCK (Y-27632, 10 µM), non-muscle myosin II (Blebbistatin, 50 µM), and FAK (PF-573228, 10 µM) were used. For inhibition of actin filaments, small molecule antagonists of polymerization (Cytochalasin D, 1 µM) and depolymerization (Jasplakinolide, 0.1 µM) were used. For inhibition of microtubules, a depolymerization agonist (Nocodazole, 10 µM) was used. For the inhibition of PI3K, a small molecule antagonist (LY294002, 20 µM) was used. For inhibition of BMP Type 1 Receptor (BMPR1), a small molecule antagonist (LDN-193189, 0.1 µM) was used. All inhibitors were purchased from Cayman Chemical and dissolved in dimethyl sulfoxide (DMSO).

STATISTICAL ANALYSIS

Statistical analysis of sequencing datasets is described in the respective methods sections. All other statistical analyses were conducted using GraphPad Prism 10.4. All statistical tests performed for analysis are described in each respective figure caption.

ACKNOWLEDGMENTS

We thank members of the Stowers lab for critical feedback on this manuscript. Additionally, we thank Ben Lopez for essential guidance in imaging and gel cryosectioning instrumentation. We acknowledge the use of the NRI-MCDB Microscopy Facility at the University of California, Santa Barbara. Furthermore, we acknowledge the use of the Biological Nanostructures Laboratory within the California NanoSystems Institute, supported by the University of California, Santa Barbara, and the University of California, Office of the President. I.M.T. and A.Z. were supported by the California Institute for Regenerative Medicine (CIRM) COMPASS EDUC5-13744 training grant. A.S. was supported by the CIRM EDUC4-12821 training grant.

REFERENCES

Beederman M, Lamplot JD, Nan G, Wang J, Liu X, Yin L, Li R, Shui W, Zhang H, Kim SH, *et al.* (2013). BMP signaling in mesenchymal stem cell differentiation and bone formation. J Biomed Sci Eng 6, 32–52.

Boergermann JH, Kopf J, Yu PB, Knaus P (2010). Dorsomorphin and LDN-193189 inhibit BMP-mediated Smad, p38 and Akt signalling in C2C12 cells. Int J Biochem Cell Biol 42, 1802–1807.

Charbonier F, Indana D, Chaudhuri O (2021). Tuning viscoelasticity in alginate hydrogels for 3D cell culture studies. Curr Protoc 1, e124.

Chaudhuri O, Gu L, Klumpers D, Darnell M, Bencherif SA, Weaver JC, Huebsch N, Lee H, Lippens E, Duda GN, *et al.* (2016). Hydrogels with tunable stress relaxation regulate stem cell fate and activity. Nat Mater 15, 326–334.

Chen JC, Jacobs CR (2013). Mechanically induced osteogenic lineage commitment of stem cells. Stem Cell Res Ther 4, 107.

Comisar WA, Kazmers NH, Mooney DJ, Linderman JJ (2007). Engineering RGD nanopatterned hydrogels to control preosteoblast behavior: a combined computational and experimental approach. Biomaterials 28, 4409–4417.

Darnell M, Gu L, Mooney D (2018a). RNA-seq reveals diverse effects of substrate stiffness on mesenchymal stem cells. Biomaterials 181, 182–188.

Darnell M, O'Neil A, Mao A, Gu L, Rubin LL, Mooney DJ (2018b). Material microenvironmental properties couple to induce distinct transcriptional programs in mammalian stem cells. Proc Natl Acad Sci USA 115, E8368–E8377.

Darnell M, Young S, Gu L, Shah N, Lippens E, Weaver J, Duda G, Mooney D (2017). Substrate stress-relaxation regulates scaffold remodeling and bone formation in vivo. Adv Healthcare Mater 6, 1601185.
Deng P, Chang I, Wang J, Badreldin AA, Li X, Yu B, Wang C-Y (2022). Loss of KDM4B impairs osteogenic differentiation of OMSCs and promotes oral bone aging. Int J Oral Sci 14, 1–11.
Di-Luoffo M, Ben-Meriem Z, Lefebvre P, Delarue M, Guillermet-Guibert J (2021). PI3K functions as a hub in mechanotransduction. Trends Biochem Sci 46, 878–888.
Downing TL, Soto J, Morez C, Houssin T, Fritz A, Yuan F, Chu J, Patel S, Schaffer DV, Li S (2013). Biophysical regulation of epigenetic state and cell reprogramming. Nat Mater 12, 1154–1162.
Duan Z, Lu H (2021). Effect of mechanical strain on cells involved in fracture healing. Orthop Surg 13, 369–375.
Engler AJ, Sen S, Sweeney HL, Discher DE (2006). Matrix elasticity directs stem cell lineage specification. Cell 126, 677–689.
Franceschi RT, Xiao G, Jiang D, Gopalakrishnan R, Yang S, Reith E (2003). Multiple signaling pathways converge on the Cbfa1/Runx2 transcription factor to regulate osteoblast differentiation. Connect Tissue Res 44, 109–116.
Fujita T, Azuma Y, Fukuyama R, Hattori Y, Yoshida C, Koida M, Ogita K, Komori T (2004). Runx2 induces osteoblast and chondrocyte differentiation and enhances their migration by coupling with PI3K-Akt signaling. J Cell Biol 166, 85–95.
Görlitz S, Brauer E, Günther R, Duda GN, Knaus P, Petersen A (2024). Temporal regulation of BMP2 growth factor signaling in response to mechanical loading is linked to cytoskeletal and focal adhesion remodeling. Commun Biol 7, 1–13.
Gunn SA, Kreps LM, Zhao H, Landon K, Ilacqua JS, Addison CL (2022). Focal adhesion kinase inhibitors prevent osteoblast mineralization in part due to suppression of Akt-mediated stabilization of osterix. J Bone Oncol 34, 100432.
Hashimshony T, Senderovich N, Avital G, Klochendler A, de Leeuw Y, Anavy L, Gennert D, Li S, Livak KJ, Rozenblatt-Rosen O, *et al*. (2016). CEL-Seq2: sensitive highly-multiplexed single-cell RNA-Seq. Genome Biol 17, 77.
Heo CH, Yeo KB, Chae M, Bak SY, Choi HJ, Jeong S, Choi N, Kang S-K, Jun SH, Ok M-R, *et al*. (2025). Spontaneous bone regeneration achieved through one-step alignment of human mesenchymal stem cell-embedded collagen. Acta Biomaterialia 196, 136–151.
Heo S-J, Thakur S, Chen X, Loebel C, Xia B, McBeath R, Burdick JA, Shenoy VB, Mauck RL, Lakadamyali M (2023). Aberrant chromatin reorganization in cells from diseased fibrous connective tissue in response to altered chemomechanical cues. Nat Biomed Eng 7, 177–191.
Heo S-J, Thorpe SD, Driscoll TP, Duncan RL, Lee DA, Mauck RL (2015). Biophysical regulation of chromatin architecture instills a mechanical memory in mesenchymal stem cells. Sci Rep 5, 16895.
Huang B, Li G, Jiang XH (2015). Fate determination in mesenchymal stem cells: a perspective from histone-modifying enzymes. Stem Cell Res Ther 6, 35.
Huang D, Li Y, Ma Z, Lin H, Zhu X, Xiao Y, Zhang X (2023). Collagen hydrogel viscoelasticity regulates MSC chondrogenesis in a ROCK-dependent manner. Sci Adv 9, eade9497.
Huebsch N, Arany PR, Mao AS, Shvartsman D, Ali OA, Bencherif SA, Rivera-Feliciano J, Mooney DJ (2010). Harnessing traction-mediated manipulation of the cell/matrix interface to control stem-cell fate. Nat Mater 9, 518–526.
Hwang J-H, Byun MR, Kim AR, Kim KM, Cho HJ, Lee YH, Kim J, Jeong MG, Hwang ES, Hong J-H (2015). Extracellular matrix stiffness regulates osteogenic differentiation through MAPK activation. PLoS One 10, e0135519.
Jang M, An J, Oh SW, Lim JY, Kim J, Choi JK, Cheong J-H, Kim P (2021). Matrix stiffness epigenetically regulates the oncogenic activation of the Yes-associated protein in gastric cancer. Nat Biomed Eng 5, 114–123.
Jin Y, Liu Z, Li Z, Li H, Zhu C, Li R, Zhou T, Fang B (2022). Histone demethylase JMJD3 downregulation protects against aberrant force-induced osteoarthritis through epigenetic control of NR4A1. Int J Oral Sci 14, 1–14.
Juhl IV OJ, Merife A-B, Zhang Y, Donahue HJ (2022). Inhibition of focal adhesion turnover prevents osteoblastic differentiation through β-catenin mediated transduction of pro-osteogenic substrate. J Biomed Mater Res Part B: App Biomater 110, 1573–1586.
Kanazawa S, Okada H, Hojo H, Ohba S, Iwata J, Komura M, Hikita A, Hoshi K (2021). Mesenchymal stromal cells in the bone marrow niche consist of multi-populations with distinct transcriptional and epigenetic properties. Sci Rep 11, 15811.
Kang P, Wu Z, Huang Y, Luo Z, Huo S, Chen Q (2022). Histone H3K9 demethylase JMJD2B/KDM4B promotes osteogenic differentiation of bone marrow-derived mesenchymal stem cells by regulating H3K9me2 on RUNX2. PeerJ 10, e13862.
Katoh K (2024). Signal transduction mechanisms of focal adhesions: Src and FAK-mediated cell response. Front Biosci (Landmark Ed) 29.
Kaya-Okur HS, Janssens DH, Henikoff JG, Ahmad K, Henikoff S (2020). Efficient low-cost chromatin profiling with CUT&Tag. Nat Protoc 15, 3264–3283.
Kaya-Okur HS, Wu SJ, Codomo CA, Pledger ES, Bryson TD, Henikoff JG, Ahmad K, Henikoff S (2019). CUT&Tag for efficient epigenomic profiling of small samples and single cells. Nat Commun 10, 1930.
Killaars AR, Grim JC, Walker CJ, Hushka EA, Brown TE, Anseth KS (2019). Extended exposure to stiff microenvironments leads to persistent chromatin remodeling in human mesenchymal stem cells. Adv Sci 6, 1801483.
Killaars AR, Walker CJ, Anseth KS (2020). Nuclear mechanosensing controls MSC osteogenic potential through HDAC epigenetic remodeling. PNAS 117, 21258–21266.
Kuleshov MV, Jones MR, Rouillard AD, Fernandez NF, Duan Q, Wang Z, Koplev S, Jenkins SL, Jagodnik KM, Lachmann A, *et al*. (2016). Enrichr: a comprehensive gene set enrichment analysis web server 2016 update. Nucleic Acids Res 44, W90–W97.
Lee H, Stowers R, Chaudhuri O (2019). Volume expansion and TRPV4 activation regulate stem cell fate in three-dimensional microenvironments. Nature Communications 10, 529.
Li Q, Chen X, Li X, Jiang X, Li X, Men X, Li Y, Chen S (2025). Plexin-B2 mediates orthodontic tension-induced osteogenesis via the RhoA/F-Actin/YAP pathway. J Periodontal Res 60, 1143–1155.
Li S, Wu H, Wang F, Kong L, Yu Y, Zuo R, Zhao H, Xu J, Kang Q (2024a). Enhanced bone regeneration through regulation of mechanoresponsive FAK-ERK1/2 signaling by ZINC40099027 during distraction osteogenesis. Int J Med Sci 21, 137–150.
Li S, Zhang S, Dong S, Zhao M, Zhang W, Zhang C, Wu Z (2024b). Stiffness and BMP-2 mimetic peptide jointly regulate the osteogenic differentiation of rat bone marrow stromal cells in a gelatin cryogel. Biomacromolecules 25, 890–902.
Lin P, Lin Y, Lennon DP, Correa D, Schluchter M, Caplan AI (2012). Efficient lentiviral transduction of human mesenchymal stem cells that preserves proliferation and differentiation capabilities. Stem Cells Transl Med 1, 886–897.
Liu R-X, Gu R-H, Li Z-P, Hao Z-Q, Hu Q-X, Li Z-Y, Wang X-G, Tang W, Wang X-H, Zeng Y-K, *et al*. (2023). Trim21 depletion alleviates bone loss in osteoporosis via activation of YAP1/β-catenin signaling. Bone Res 11, 1–15.
Livak KJ, Schmittgen TD (2001). Analysis of relative gene expression data using real-time quantitative PCR and the $2-\Delta\Delta CT$ method. Methods 25, 402–408.
Lou J, Stowers R, Nam S, Xia Y, Chaudhuri O (2018). Stress relaxing hyaluronic acid-collagen hydrogels promote cell spreading, fiber remodeling, and focal adhesion formation in 3D cell culture. Biomaterials 154, 213–222.
McBeath R, Pirone DM, Nelson CM, Bhadriraju K, Chen CS (2004). Cell shape, cytoskeletal tension, and RhoA regulate stem cell lineage commitment. Dev Cell 6, 483–495.
Nam S, Stowers R, Lou J, Xia Y, Chaudhuri O (2019). Varying PEG density to control stress relaxation in alginate-PEG hydrogels for 3D cell culture studies. Biomaterials 200, 15–24.
Parekh SH, Chatterjee K, Lin-Gibson S, Moore NM, Cicerone MT, Young MF, Simon CG (2011). Modulus-driven differentiation of marrow stromal cells in 3D scaffolds that is independent of myosin-based cytoskeletal tension. Biomaterials 32, 2256–2264.
Prowse PDH, Elliott CG, Hutter J, Hamilton DW (2013). Inhibition of Rac and ROCK signalling influence osteoblast adhesion. Differentiation and mineralization on titanium topographies. PLoS One 8, e58898.
Rahman MS, Akhtar N, Jamil HM, Banik RS, Asaduzzaman SM (2015). TGF-β/BMP signaling and other molecular events: regulation of osteoblastogenesis and bone formation. Bone Res 3, 1–20.
Rajshankar D, Wang Y, McCulloch CA (2017). Osteogenesis requires FAK-dependent collagen synthesis by fibroblasts and osteoblasts. FASEB J 31, 937–953.
Rath B, Nam J, Deschner J, Schaumburger J, Tingart M, Grässel S, Grifka J, Agarwal S (2011). Biomechanical forces exert anabolic effects on

osteoblasts by activation of SMAD 1/5/8 through type 1 BMP receptor. Biorheology 48, 37–48.
Reif S, Lang A, Lindquist JN, Yata Y, Gäbele E, Scanga A, Brenner DA, Rippe RA (2003). The role of focal adhesion kinase-phosphatidylinositol 3-kinase-Akt signaling in hepatic stellate cell proliferation and type i collagen expression*. J Biol Chem 278, 8083–8090.
Rowley JA, Madlambayan G, Mooney DJ (1999). Alginate hydrogels as synthetic extracellular matrix materials. Biomaterials 20, 45–53.
Roy B, Venkatachalapathy S, Ratna P, Wang Y, Jokhun DS, Nagarajan M, Shivashankar GV (2018). Laterally confined growth of cells induces nuclear reprogramming in the absence of exogenous biochemical factors. PNAS 115, E4741–E4750.
Roy B, Yuan L, Lee Y, Bharti A, Mitra A, Shivashankar GV (2020). Fibroblast rejuvenation by mechanical reprogramming and redifferentiation. PNAS 117, 10131–10141.
Sordella R, Jiang W, Chen G-C, Curto M, Settleman J (2003). Modulation of Rho GTPase signaling regulates a switch between adipogenesis and myogenesis. Cell 113, 147–158.
Stowers RS, Shcherbina A, Israeli J, Gruber JJ, Chang J, Nam S, Rabiee A, Teruel MN, Snyder MP, Kundaje A, *et al.* (2019). Matrix stiffness induces a tumorigenic phenotype in mammary epithelium through changes in chromatin accessibility. Nat Biomed Eng 3, 1009–1019.
Sun B, Qu R, Fan T, Yang Y, Jiang X, Khan AU, Zhou Z, Zhang J, Wei K, Ouyang J, *et al.* (2021). Actin polymerization state regulates osteogenic differentiation in human adipose-derived stem cells. Cell Mol Biol Lett 26, 15.
Taubenberger AV, Woodruff MA, Bai H, Muller DJ, Hutmacher DW (2010). The effect of unlocking RGD-motifs in collagen I on pre-osteoblast adhesion and differentiation. Biomaterials 31, 2827–2835.
Urist MR (1997). Bone morphogenetic protein: the molecularization of skeletal system development. J Bone Mineral Res 12, 343–346.
Walewska A, Janucik A, Tynecka M, Moniuszko M, Eljaszewicz A (2023). Mesenchymal stem cells under epigenetic control – the role of epigenetic machinery in fate decision and functional properties. Cell Death Dis 14, 720.
Wan W, Zhang H, Niu L, Zhang M, Xu F, Li A, Pei D, Lin M, Cheng B (2024). TGF-β1 promotes osteogenesis of mesenchymal stem cells via integrin mediated mechanical positive autoregulation. iScience 27, 110262.
Woloszyk A, Tuong ZK, Perez L, Aguilar L, Bankole AI, Evans CH, Glatt V (2022). Fracture hematoma micro-architecture influences transcriptional profile and plays a crucial role in determining bone healing outcomes. Biomater Adv 139, 213027.
Wu M, Chen G, Li Y-P (2016). TGF-β and BMP signaling in osteoblast, skeletal development, and bone formation, homeostasis and disease. Bone Res 4, 1–21.
Wu Y, Song Y, Soto J, Hoffman T, Lin X, Zhang A, Chen S, Massad RN, Han X, Qi D, *et al.* (2025). Viscoelastic extracellular matrix enhances epigenetic remodeling and cellular plasticity. Nat Commun 16, 4054.
Xu H, Wu F, Zhang H, Yang C, Li K, Wang H, Yang H, Liu Y, Ding B, Tan Y, *et al.* (2017). Actin cytoskeleton mediates BMP2-Smad signaling via calponin 1 in preosteoblast under simulated microgravity. Biochimie 138, 184–193.
Xu J, Yu B, Hong C, Wang C-Y (2013). KDM6B epigenetically regulates odontogenic differentiation of dental mesenchymal stem cells. Int J Oral Sci 5, 200–205.
Ye L, Fan Z, Yu B, Chang J, Al Hezaimi K, Zhou X, Park N-H, Wang C-Y (2012). Histone demethylases KDM4B and KDM6B promotes osteogenic differentiation of human MSCs. Cell Stem Cell 11, 50–61.
Ying Q, Jiang Y, Sun C, Zhang Y, Gao R, Liu H, Liu H, Guo J, Li M (2024). AGEs impair osteogenesis in orthodontic force-induced periodontal ligament stem cells through the KDM6B/Wnt self-reinforcing loop. Stem Cell Res Ther 15, 431.
Zhao X, Guan J-L (2011). Focal adhesion kinase and its signaling pathways in cell migration and angiogenesis. Adv Drug Delivery Rev 63, 610–615.
Zhou J, Lee P-L, Lee C-I, Wei S-Y, Lim SH, Lin T-E, Chien S, Chiu J-J (2013). BMP receptor-integrin interaction mediates responses of vascular endothelial Smad1/5 and proliferation to disturbed flow. J Thromb Haemost 11, 741–755.
Zhu S, Chen W, Masson A, Li Y-P (2024). Cell signaling and transcriptional regulation of osteoblast lineage commitment, differentiation, bone formation, and homeostasis. Cell Discov 10, 1–39.